JMEPEG (1997) 6:289-299

Evaluation of the Nucleation and Coarsening Kinetic Behavior of the Secondary Hardening Carbide of Fe-14Co-10Ni-1Mo-0.16C Steel at Two Chromium Levels, Using an Analytical and Modeling Approach: Part II

Y. Oh, P.M. Machmeier, T. Matuszewski, and R. Ayer

The effect of 1% Cr addition on the resistivity during preaging and peak aging of an AF1410 based steel was examined by analytical and modeling approaches. The increased kinetics of aging resulting from a chromium addition, due to a variety of complex microstructural changes, was analyzed by Avrami-Mehl and Wert-Zener formulations, which were modified so that the exponent was a function of time. Using a generalized Avrami equation, it was shown that the nucleation rate, $N(t)$, at short aging times was large but became a rapidly declining function as $N(t)$ approaches zero in a supersaturated system. A mathematical solution, using AF1410 steel carbide growth data at 510 °C, confirmed reported experimental evidence of second-stage carbide nucleation at 1 to 2 h.

Keywords
kinetics of aging, property modeling, steel properties

1. Introduction

IN THE DEVELOPMENT of a series of AF1410 based secondary hardening steels in high-performance Fe-Co-Ni-Cr-Mo-C steels, Machmeier et al. (Ref 1, 2) reported accelerated aging when chromium was increased from 2 to 3 wt%. This behavior is investigated by data analysis and modeling as a background for an improved understanding of the thermal treatment and mechanical property optimization (Ref 3). Earlier work by Chandhok et al. (Ref 4, 5) disclosed that, in high strength steels, the addition of cobalt maintained a high dislocation density by retarding the recovery of the dislocation substructure. Later, Speich et al. (Ref 6) confirmed this behavior and reported a chromium-related peak hardness shift for Fe-Ni-Co-Cr-Mo-C secondary hardening steels.

The M_2C secondary hardening reaction in steel was investigated previously (Ref 6, 7), but only recently did the importance of this phenomenon become recognized in commercial steels. It was not resolved by transmission electron microscopy (TEM) whether the molybdenum-rich zones, which preceded the precipitation of the fine needles of M_2C (Ref 7, 8) can cause streaking. The field ion microscopy (FIM) examination in conjunction with atom probe (AP) microanalysis (Ref 9-11) of the AF1410 steel, aged for approximately 100 s at 510 °C, revealed small clusters prior to the precipitation of fine needle M_2C carbides. Olson and others (Ref 11-13) proved that molybdenum initially forms M_2C carbides as a result of the higher driving force. Chromium diffuses in and out of this carbide structure as equilibrium is approached. Heterogeneous nucleation of M_2C carbides occurs on a highly dislocated substructure as defined by Olson (Ref 14) and Speich et al. (Ref 6). Ayer et al. (Ref 3, 8) systematically demonstrated by strain contrast that as the M_2C carbides coarsen and approach optimum strength, they displayed carbide and matrix coherency, thus invoking Orowan looping.

The isothermal aging response of the experimental AF1410 series steels appears to be complex as experimental evidence suggests the nucleation and diffusion-controlled coarsening process will be interrupted. Cementite is precipitated initially and at a later stage is resolutionized. Retained austenite will transform, and later, reverted austenite may appear depending on the temperature of aging. The sequence of the M_2C formation and other microstructural characterization is discussed in a companion paper (Ref 15). In this article, the nucleation and growth kinetics of the two alloys, the 14Co-10Ni-1Mo-0.16C steels with 2 and 3% Cr, respectively, are investigated for aging temperature ranging from 454.4 to 537.8 °C for 6 min to 60×10^3 min (1000 h).

In the investigation of the coarsening and nucleation analysis, there are two competing theories, namely, the Avrami-Johnson-Mehl formulation (Ref 16-19) and the Wert-Zener formulation (Ref 20). Even though they were used extensively in the past, the precise nature of the relationship between the two theories is not clear. In this study, the Wert-Zener equation is solved for a closed-form solution; thereby, they can be compared. It turns out that the Wert-Zener equation is a type of Avrami relationship with the "asymptotic" exponent of 1.0. The Avrami formula is well suited for most experimental studies, even though the exponent n is not necessarily a constant. Instead of using a constant exponent, the original Avrami formula is generalized so that not only a constant, but any function can be substituted for the exponent n. Moreover, the average exponent n values obtained from the experiment area about 0.2 to 0.5, which are much less than 1.0. According to the conventional Avrami formulation, the n must be greater than 1.0. For example, $n = 2.0$ for one-dimensional precipitation growth, $n = 3.0$ for two-dimensional sheet growth, and $n = 4.0$ for three-di-

Y. Oh, P.M. Machmeier, T. Matuszewski, Snap-On Tools Inc., Kenosha, WI, USA; **R. Ayer,** STEM, Woodbridge, CT, USA.

mensional spherical growth (Ref 21). This requires a closer examination of the basic Avrami formulation.

By further generalization of the Avrami Formula, the growth and nucleation rate functions are combined, and their relationship is explicitly disclosed. To solve the nucleation behavior of the precipitation process, additional data are needed. The microstructure evolution data satisfies this requirement, that is, the average growth pattern of the particle. By using this evolution data along with the resistivity measurements, the nucleation rate function can be solved.

2. Procedure

2.1 *Experimental*

The nucleation and growth kinematics of steel compositions 14Co-10Ni-1Mo-0.16C with 2% Cr (AF1410) and the 14Co-10Ni-1Mo-0.16C with 3% Cr were studied by resistivity for temperatures ranging from 454.4 to 537.8 °C and times from 6 to 6×10^3 min. The $5.08 \times 3.94 \times 85.75$ mm resistivity specimens were thermally treated in an experimental furnace in which ±2 °C were maintained by specimen thermocouples. A collinear four-probe array (59.95 and 76.20 mm between potential and current probes) with a constant load of 2.83 kg was applied to the sample holder at ambient temperature during all measurements. Corrections and checks were made for temperature, current direction, and specimen heating. A constant voltage source was used, and voltages were read to a ±1 MV sensitivity when the current was less than 1 A. The determined error for all resistivity readings was less than ±1.0%. The resistivity data ρ(MΩ-cm) are used to determine the volume fraction transformed, w, from the following formula:

$$w = (\rho_0 - \rho)/(\rho_0 - \rho_\infty) \quad \text{(Eq 1)}$$

where ρ_0 is resistivity at 0.0 min 0.5560 μΩ-m as quenched for 2% Cr, 0.6448 μΩ-m as quenched for 3% Cr, ρ_∞ is resistivity at 60×10^3 min, and ρ is instantaneous value of resistivity.

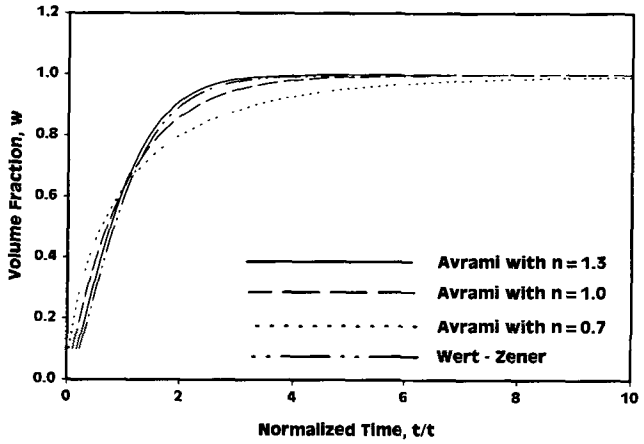

Fig. 1 Comparison of Avrami-Johnson-Mehl versus Wert-Zener formulas

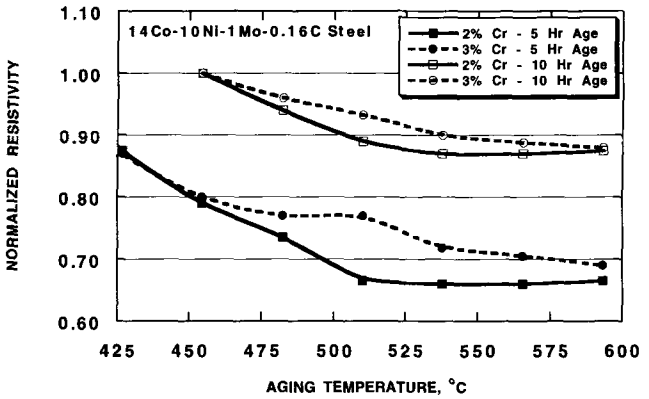

Fig. 2 Variation of resistivity during aging of 14Co-10Ni-1Mo-0.16C steel

2.2 *Analytical*

In the study of the coarsening phenomenon, the most frequently used formula is Avrami-Johnson-Mehl equations (Ref 16-19):

$$w = 1 - \exp\left[-\left(\frac{t}{\tau}\right)^n\right] \quad \text{(Eq 2)}$$

where w is the volume fraction transformed, t is time, τ is a time constant, and n is an exponent presumed to be a constant. These values w, τ, and n are often obtained experimentally from the resistivity or hardness data.

There is another competing theory proposed by Wert-Zener (Ref 20). However, the formula is given in terms of a differential equation:

$$\tau \frac{dw}{dt} = \frac{3}{2}[(1-w)w^{1/3}] \quad \text{(Eq 3)}$$

rather than a closed-form solution like the Avrami relationship. Therefore, it is difficult to compare the two theories, much less to choose the appropriate formulation for a particular experiment at hand. However, the Wert-Zener equation can be solved explicitly so that the two formulas can be compared. By changing the variable, $y = w^{1/3}$ and simplifying both sides of the equation (Eq 3), it is shown:

$$\frac{y}{1-y^3}dy = \frac{1}{2\tau}dt \quad \text{(Eq 4)}$$

Then integrating both sides:

$$\frac{t}{\tau} = \frac{2}{3}\ln\left[\frac{\sqrt{w^{2/3}+w^{1/3}+1}}{(1-w^{1/3})}\right] - \frac{2}{\sqrt{3}}\arctan\left[\frac{(2w^{1/3}+1)}{\sqrt{3}}\right] + 0.6046 \quad \text{(Eq 5)}$$

which is an analytical solution of the Wert-Zener equation.

The Avrami formula can also be written in a similar manner expressing t in terms of w, as follows:

$$t/\tau = \{\ln[1/(1-w)]\}^{1/n} \quad \text{(Eq 6)}$$

It is not obvious how one formula is related to the other as shown in Fig. 1. At an n of 1.0 to 1.3, there is closer agreement to the Wert-Zener relationship, especially as $w < 0.7$. However, the difference becomes more pronounced as w approaches 1.0 or time (t) becomes larger.

3. Experimental Results

3.1 *Aging Kinetics*

Kinetic data were obtained by measurement of the variation in resistivity with time for a series of specimens isothermally aged at various temperatures. Aging curves for 2% Cr and 3% Cr, using normalized resistivity changes measured from 427 to 593 °C, revealed that the maximum change in resistivity occurs during M_2C precipitation (Fig. 2). The differences in resistivity represent complex reactions where M_3C forms and is resolutionized, retained γ is transformed, reverted γ is nucleated, coherency strains exist, and M_2C carbides are formed. Isothermal aging curves using a generalized Johnson-Mehl-Avrami relationship (Eq 2) are shown in Fig. 3 and 4. In both alloys, the reaction ($w \rightarrow 1$) was not compete at 100 h, Fig. 5. Near equilibrium conditions were obtained at 6×10^4 min.

The plot revealed that the time exponents are considerably <1.0 and tend to be discontinuous after 300 min. TEM analysis revealed that the addition of 3% Cr increases the dissolution kinetics of Fe_3C in the 454 to 482 °C age range (Ref 1, 3, 8, 15). The work also showed that Fe_3C does not readily form in the 3% Cr composition; thus carbon is readily available for rapid M_2C precipitation at dislocation nucleation sites. It is clear from Fig. 3 and 4 that the early nucleation of carbide clusters and the coarsening of M_2C carbides result in low slopes (n = 0.2 to 0.4), which are lower than slope estimates previously projected by theory or experiment. This slope range at 510 °C holds for the 2% Cr steel up to $w = 0.738$ and the 3% Cr steel up to $w = 0.675$, where a slope change coincides with the resolutionized Fe_3C and the formation of reverted austenite. The kinetics of Mo_2C alloy carbide formation in martensite, during aging treatments, by Wilkes (Ref 21) (n = 1.0 to 0.5, later stage) and Derbyshire-Barford (Ref 22) (n = 0.65) indicate that the kinetics of reaction are somewhat faster than observed in the AF1410 based steels. An explanation is that the high aging temperature (>500 °C) resulted in increased diffusion rates and some microstructural recovery. In cases where low dislocation density bainitic structures were run for comparison, there was a decrease in nucleation rate leading to a higher n value. To account for the decreased n in the 2 and 3% Cr steels, the authors speculated that the increased nucleation rate of M_2C type clusters at the dislocations lead to w values greater than 0.41 at 482 to 537 °C (Fig. 3 and 4). Thus, the slope of the modified Avrami curves (ln ln $1/(1-w)$ vs. ln t) deals primarily with short-range solute diffusion or coarsening, even though nucleation is predicted to occur up to 120 min. In other experimental work, Murphy and Whiteman (Ref 23) revealed that the formation of Mo_2C carbide in tempered martensite can be described at 520 °C by n of 0.67 from a w of ≈0 to 0.65, where a sharp change in slope suggests a change in the mechanism of carbide transformation. At approximately 300 min, the mean length of Mo_2C needles vary from 20 to 30 nm (Ref 8, 26) in the 2% Cr steel, and it was shown that the M_2C retains a higher level of molybdenum resulting in higher hardness.

The volume of Fe_3C is less when coupled with the increased dissolution kinetics (Ref 24), which effectively separated the Fe_3C reaction from the M_2C carbide. The variation in the precipitation of the M_3C and M_2C type curves at 2 and 3% Cr levels is depicted in Fig. 6 and 7.

4. Comparison of Avrami Versus Wert-Zener Models

If the transformation curves are broken into two segments of $w < 0.7$ and $w > 0.7$, it appears that the Wert-Zener formulation

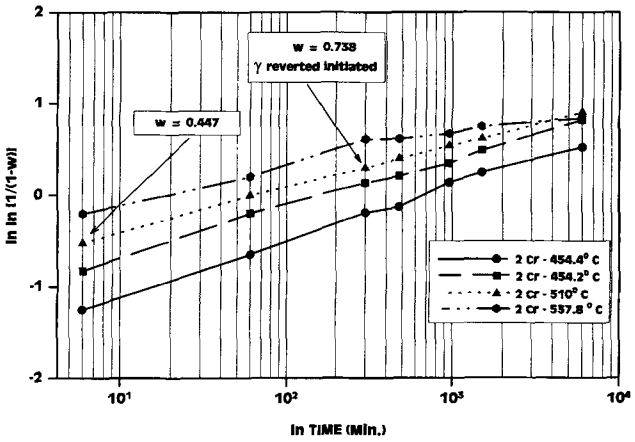

Fig. 3 Isothermal precipitation for the 2%Cr alloy: ln ln $[1/(1-w)]$ versus ln time

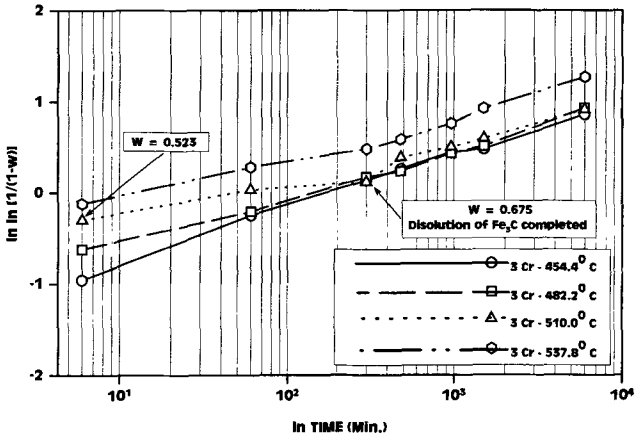

Fig. 4 Isothermal precipitation for the 3%Cr alloy: ln ln $[1/(1-w)]$ versus ln time

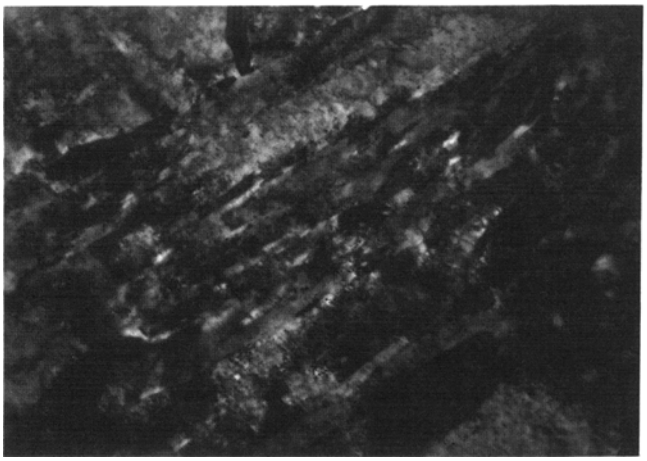

(a)

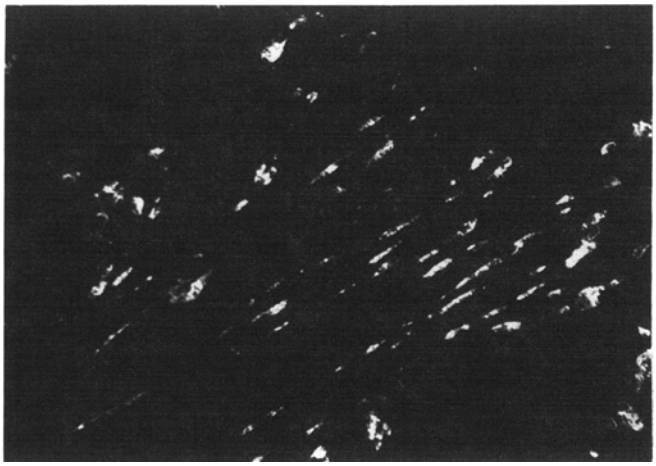

(b)

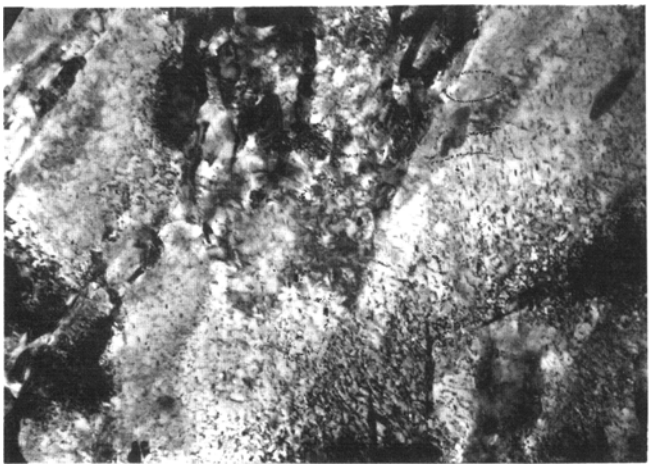

(c)

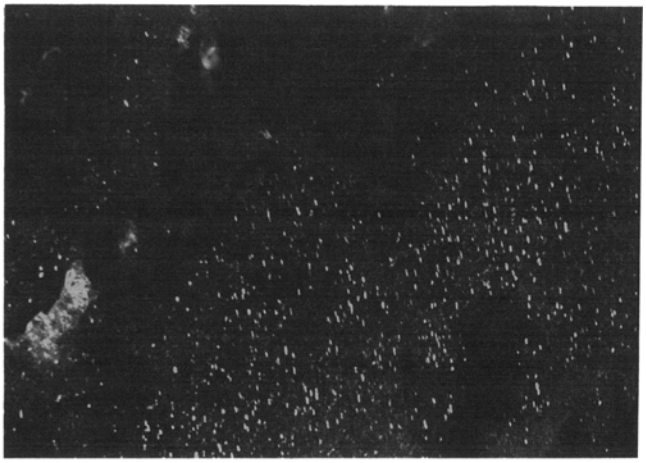

(d)

Fig. 5 2% Cr steel: Fe-14Co-10Ni-1Mo-0.16C aged 510 °C for 100 h. (a) Partially recovered substructure, 22,000×. (b) Dark field, 8 vol% γ, 22,000×. (c) Overaged M_2C precipitates, 22,000×. (d) Dark field image, M_2C needles, 7.0 nm diam, 35 nm long, 22,000×

predicts behavior satisfactorily, as $w \approx 1.0$ and a long period of time, $t \approx \infty$.

Then:

$$\frac{t}{\tau} \approx \frac{2}{3} \ln\left[\sqrt{\frac{1+1+1}{(1-w^{1/3})}}\right] - \frac{2}{\sqrt{3}} \arctan\left[\frac{(2+1)}{\sqrt{3}}\right] + 0.6046 = \frac{2}{3} \ln\left[\frac{1}{(1-w^{1/3})}\right] - 0.2384 \quad \text{(Eq 7)}$$

Solving for $w^{1/3}$, it follows that:

$$w^{1/3} = 1 - 0.699 \exp\left[-1.5\,(t/\tau)\right] \quad \text{(Eq 8)}$$

By simplifying and maintaining only the most dominant component as $(t \rightarrow \infty)$ and disregarding the rest, the authors have:

$$w = 1 - 2.097 \exp\left[-1.5\,(t/\tau_1)^{1.0}\right] \text{ where } (t = \tau/1.5) \quad \text{(Eq 9)}$$

When comparing the above formula with the Avrami formula (Eq 2):

$$w = 1 - \exp\left[-(t/\tau)^n\right]$$

it can be seen that the Wert-Zener formula is a kind of Avrami formula with the exponent $n = 1.0$ when w is close to ≈1.0 as time approaches $t \approx \infty$. Of course, when w is not close to 1.0 or time (t) is not large, the Wert-Zener and Avrami-Johnson-Mehl formulations are not easily compared. Also n is not always a constant in this relationship. See Appendix 1 for the solution that yields:

$$w(t) = 1 - \exp\left[-t^m/\tau'\right] \text{ where } \tau' = \exp(-b) \quad \text{(Eq 10)}$$

Figure 8 shows that the modified solution fits the experimental resistivity data better than the conventional Avrami formulation.

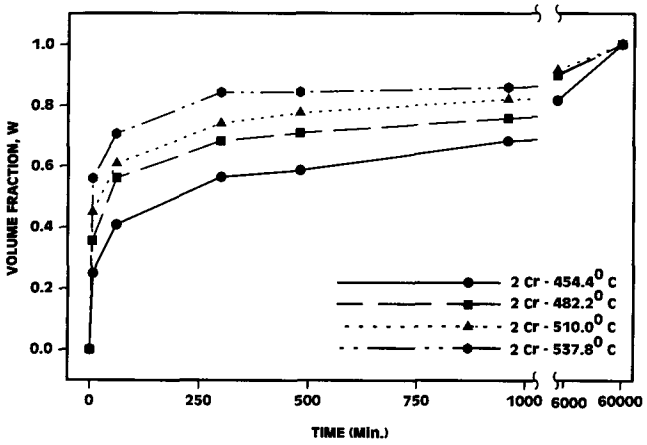

Fig. 6 Transformation curves for precipitation of M_3C and M_2C type carbides at different aging temperatures for the 2%Cr steel

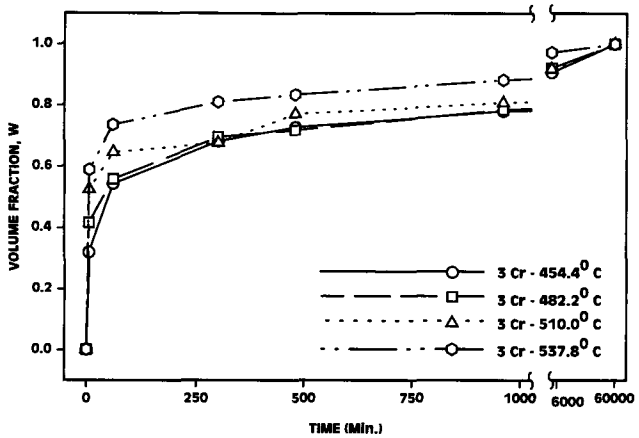

Fig. 7 Transformation curves for precipitation of M_3C and M_2 type carbides at different aging temperatures for the 3%Cr steel

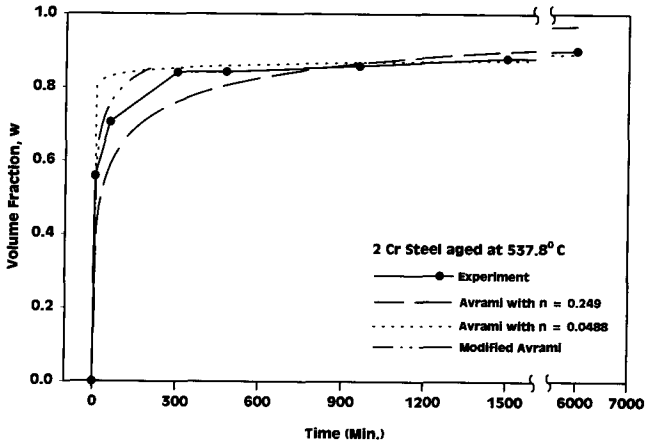

Fig. 8 Comparison of a modified Avrami formula with experimental transformation data

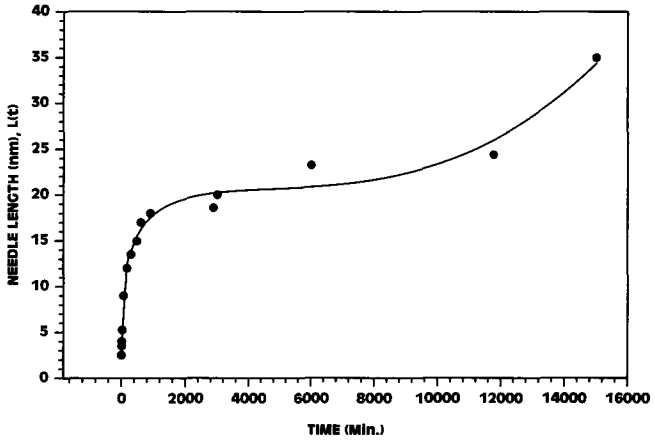

Fig. 9 Averaged M_2C type precipitate length in the 2%Cr steel (AF1410) at 510 °C

5. Nucleation Rate

Previous investigations revealed the rapid nucleation rate of these alloys at apparent dislocation sites (Ref 9-11). While it is expected that the chromium content may strongly affect the nucleation kinetics, growth data for the 3% Cr alloy in this range is not available. Thus, AF1410 steel (2% Cr) cluster-carbide coarsening data, during aging at 510 °C from 0.9 to 1.5×10^4 min, is compiled in Table 1.

A basic kinetic equation (Ref 28) can be used to describe the nucleation and coarsening of particles precipitated during isothermal aging as:

$$w = 1 - \exp\left[-(t/\tau)^n\right] = 1 - \exp\left[-\int_0^t N(s)V(t-s)ds\right] \quad \text{(Eq 11)}$$

where w is the volume fraction transformed in time t, N is the nucleation frequency, $V(t-s)$ is the particle volume nucleated at time $(t - s)$, and s is a "dummy" variable in the convolution type integral.

The assumptions are that the particles are randomly nucleated and grow randomly from each other in the martensite matrix. In a short form of Eq 11, the generalized Avrami formula yields:

$$\int_0^t N(s)V(t-s)ds = \left(\frac{t}{\tau}\right)^n \quad \text{(Eq 12)}$$

This formula combines the three functions, the time-exponent $(t/\tau)^n$, the nucleation rate function $N(s)$, and the particle volume growth function $V(s)$. If any two of the three functions are known, then the third function can be found, at least in principle. $N(s)$ is solved for a discrete solution, as the closed form is not solvable.

First, from the resistivity measurement, $(t/\tau)^n$ can be determined by using the usual ln ln $1/(1 - w)$ versus ln t curve as before. Second, from the microstructure evolution data, the

pattern of the volume growth $V(s)$ can be determined provided that the coarsening particles maintain a consistent geometric shape throughout the evolution period. From the resistivity data on 2% Cr at 510 °C, it follows that:

$$(t/\tau)^n = (t/70.78)^{0.207} \quad \text{(Eq 13)}$$

where time t is in minutes.

Because the basic particle form is assumed to be a needle shape, the volume of each particle can be expressed as a function of time:

$$V(t) = A_0 L(t) \quad \text{(Eq 14)}$$

where A_0 = average cross-sectional area of the "needle," relatively constant, and $L(t)$ = length of the needle at the time t, a predominant variable.

Table 1 records the needle growth for time t ranging from $t = 0.9$ min through $t = 15{,}000$ min. These data determine the value of $L(t)$ at those specified times in Table 1, and for other time instances, the approximated curve is used as shown in Fig. 9.

The integral in Eq 11 can be solved for $N(s)$ by a Riemannian summation in Appendix 2. A set of n equations is formulated by dividing the interval $[0,t]$ in many Δt subintervals that can be put into a matrix form and solved. A simulated nucleation rate function for the carbide data in Fig. 9 from the solution of the generalized Avrami Eq 11 by the matrix solution is shown in Fig. 10. This plot is derived from the matrix solution of the M_2C carbide length data, which is substituted into the Avrami integral (Eq 12).

A good approximation can be obtained from a closed loop solution when t is close to 0 at $1/t^n$.

By substituting a length function (curve fitting algorithm [Table 3 data]) into the integral (Eq 11):

$$A_0 \int_0^t N(s)[4.303442\,(t-s)^{-1} - 6.7902\,(t-s)^{-1.5}]$$
$$ds = 0.207\,\tau^{-1}\,(t/\tau)^{-0.793} \quad \text{(Eq 15)}$$

where:

$$A_0 N(s) = A + Bs^{-0.793} + Cs^{-0.293} = 0.543413 - 0.207097s^{-0.793} + 0.32792s^{-0.293} \quad \text{(Eq 16)}$$

The best fit solution in Fig. 10 indicates that the nucleation rate function is rapidly decreasing as the beginning approaches zero. Therefore, after a short time, there are few nucleation sites generated. The actual amount of nuclei is the area under the nucleation rate curve, which can be obtained by performing an integration of the rate function. The rate of embryo nucleation from a supersaturated solution varies from extremely rapid to a reduced value, passing through a range of supersaturations (Ref 29, 30).

Further studies of the competition between the nucleation and growth of γ' precipitates in nickel (Ref 31), disclosed that the Langer-Schwartz theory had to be modified to interpret the decrease of nucleation embryos to allow for Ostwald ripening.

Note that the nucleation rate $N(t)$, thus calculated, is not a "genuine" nucleation rate any longer because in the multicomponent experiment, the carbides of different types are emerging and disappearing throughout the entire coarsening process. Also, it is highly unlikely that the nucleation is homogeneous but rather a heterogeneous event at dislocation sites (Ref 11). Therefore, the solution obtained is an average of many complicated events. It would be difficult to derive any definite conclusions from this solution for the multicomponent coarsening.

However, this solution provides an interesting nucleation pattern. For example, the nucleation rate is hardly a constant as assumed in the derivation of the usual Avrami formula. It is suspected that the nucleation rate at time ($t \approx 0$) may be ex-

Table 1 AF1410 steel growth data, 2% Cr M_2C carbides at 510 °C

Time, min	Average length, nm	Measured length, nm		
		Ref 25	Ref 26	Ref 27
0.9	2.5	...	...	2.5
4.98	2.5	...	...	2.5
6.0	2.5	...	2.5	...
15.0	4.0	...	...	4.0
18.0	3.5	...	3.5	...
30.0	5.25	...	5.0	5.5
60.0	9.0	...	9.0	9.0
180.0	12.0	...	12.0	12.0
300.0	13.5	...	15.0	12.0
480.0	14.95	11.9	...	18.0
600.0	17.0	...	17.0	...
900.0	18.0	...	18.0	...
960.0	19.45	13.9	...	25.0
2,880.0	18.6	18.6	...	...
3,000.0	20.0	...	20.0	...
6,000.0	23.25	21.5	25.0	...
11,760.0	24.4	24.4	...	...
15,000.0	35.0	...	35.0	...

tremely large and becomes a rapidly decreasing function as $N(t)$ approaches zero (Fig. 10). At this point, there is speculation that some resolutionizing of the nuclei occurs at a given rate during ripening, prior to precipitate growth.

Also of interest in the 2% Cr (AF1410) steel, is the reported second stage of nucleation between 1 and 2 h that follows a short growth period (Ref 11, 14). This behavior has not been reported in the 3% Cr steels during APFM analysis.

It is known that the fine M_2C type carbides, which are precipitated from supersaturated solid solutions, will initially grow at the expense of matrix solutes. The nucleation duration was reported from 6 to 120 min. The ability of the multicomponent carbides $(Mo_y, Cr_y)_xC$ to adjust composition to achieve an evolving compromise between interfacial energy and volume driving force may be an important factor in sustaining the nucleation (Ref 11). To evaluate this premise, the M_2C carbide length, at 510 °C for the AF1410 steel, is expressed as $f(t) = \ln [1/(1 - w)]$ using the modified Avrami curves [$\ln 1/(1 - w)$ versus $\ln t$] in Fig. 3 to fit the growth data (Fig. 11). This relationship was substituted into the generalized Avrami nucleation rate relationship (Eq 11), where after many corrective interactions for $w = f(t)$, evidence of a primary and secondary carbide nucleation event occurs as reported in previous experimental work (Ref 14) (Fig. 12).

6. Discussion

The addition of 1% Cr to the Fe-14Co-10Ni-2Cr-1Mo-0.16C steel (AF1410) substantially increased the isothermal aging kinetics of this system as measured by resistivity. Increased chromium limits the formation of autotempered cementite (Ref 15), which caused a marked decrease in the coarsening rate of cementite particles during aging (Ref 24) and decreases the stability of cementite, leading to the early formation of M_2C carbides (Ref 8). It was suggested that the coarsening of the M_3C and M_2C series of carbides is related to the rate controlling step of chromium diffusion (Ref 32). In a supersaturated matrix, high molybdenum has a large driving force to form M_2C; however, this is counteracted by the diffusion of chromium in the $(Mo_{1-x}Cr_x)_2C$ carbide, which results in a decreased lattice parameter (Ref 15). The reduced critical particle size for particle shear versus Orowan looping moves the peak hardness to a lower temperature during secondary hardening (Ref 13, 14).

In this study, the two main theories of the precipitation phenomena, namely the Avrami-Johnson-Mehl and Wert-Zener formulations, are reexamined and compared from a computational perspective. They are not exactly identical to each other, but it is found that Wert-Zener is a kind of Avrami formulation with the time exponent n close to 1.0. This information is helpful for choosing a "correct" theory for a particular experiment at hand.

In the experiment, the average values of the exponent n are about 0.2 to 0.5, less than 1.0. Therefore, the Avrami formulation is used throughout the study. Moreover, the n values do not remain constant, as they often vary throughout the precipitation process. For better approximation, the conventional Avrami formula is modified so that the exponent n can be any function of time. In most cases, they consist of "piecewise" linear segments.

To investigate the nucleation effect, a generalized version of Avrami is considered that relates the nucleation rate function with the growth function. To solve for the nucleation, additional data are needed, such as the microstructure evolution, which determines the pattern of the particle growth. Based on

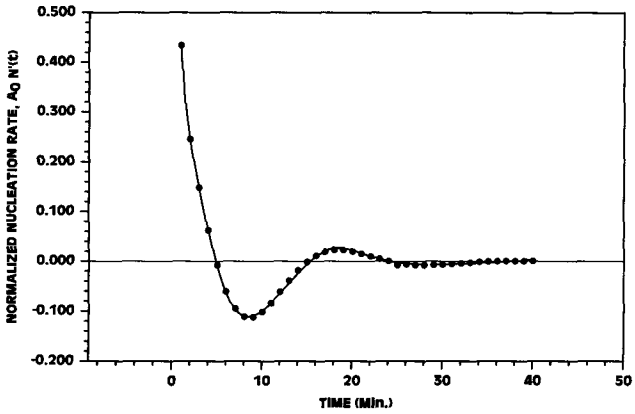

Fig. 10 Simulated nucleation rate function

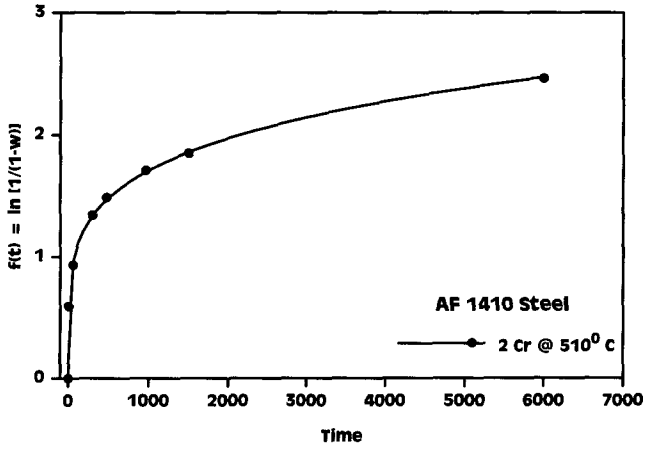

Fig. 11 Carbide needle length represented as $f(t) = \ln[1/(1 - w)]$ for resistivity data using a modified Avrami relationship

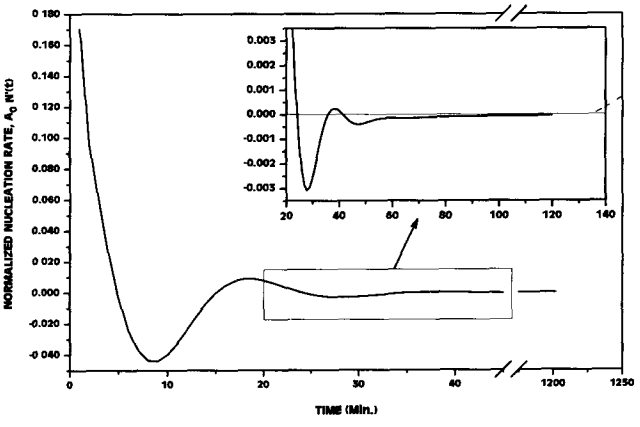

Fig. 12 Simulated second nucleation rate function

these data, the nucleation rate function can be obtained. Because the nucleation rate function is rather sensitive to the initial data, it is important to have accurate data of resistivity and growth evolution, especially when $t \approx 0$.

Because the exponent n is less than 1.0, it is expected that a singularity exists when the nucleation at $t = 0$. A further analysis was carried out to understand the nucleation behavior at the start of the precipitation process, although it is not included in this paper.

It must, however, be acknowledged that the nucleation solution, thus obtained, merely represents the "average" effect of very complicated events and different types of carbides constantly emerging and disappearing throughout the entire process. Further investigation of multicarbide component systems, especially at the early stages of nucleation, would require carefully constructed experiments.

7. Conclusions

- In AF1410 based composition steels, an addition of 1 wt% Cr resulted in an increase in the Fe_3C dissolution and kinetics of the M_2C carbide formation.
- To improve the modeling behavior of the Avrami and Wert-Zener formulations, they were modified so that the exponent n can be any function of time. The selection of the best formula depends on the time exponent and the requirement to primarily analyze the nucleation as coarsening of precipitates.
- Using a generalized Avrami equation, it was shown that the nucleation rate ($N(t)$) at time ($t \approx 0$) was large but becomes a rapidly declining function as $N(t)$ approaches zero in a supersaturated system. A mathematical solution, using AF1410 steel (2% Cr) carbide growth data at 510 °C, confirmed reported experimental evidence of second stage carbide nucleation between 0.6 and 2 h.

References

1. P.M. Machmeier, C.D. Little, M.H. Horowitz, and R.P. Oates, Development of a Strong (1650 MN/m^2) Tensile Strength Martensite Steel Having Good Fracture Toughness, *Met. Technol.*, 1979, p 291
2. C.D. Little and P.M. Machmeier, "Development of a Weldable High Strength Steel," Report AFML-TR-75-148, Wright Patterson Air Force Base, 1975
3. R. Ayer and P. Machmeier, "Microstructural Basis for the Effect of Cr on the Strength and Toughness of AF1410-Based High Steels," *Metall. Trans.*, Vol 27A, 1996, p 2510
4. V.K. Chandhok, J.P. Hirth, and E.J. Dulis, Effect of Cobalt on Tempering Tool and Alloy Steels, *Trans. ASM*, Vol 56, 1963, p 677
5. V.K. Chandhok, J.P. Hirth, and E.J. Dulis, Effect of Cobalt on Carbon Activity and Diffusivity in Steel, *Trans. AIME*, Vol 224, 1962, p 858
6. G.R. Speich, D.S. Dabkowski, and L.F. Porter, Strength and Toughness of Fe-10Ni Alloys Containing C, Cr, Mo and Co, *Metall. Trans.*, Vol 4, 1973, p 303
7. D. Raynor, J.A. Whiteman, and R.W.K. Honeycombe, Precipitation of Molybdenum and Vanadium Carbides in High-Purity Iron Alloys, *JISI*, 1966, p 349
8. R. Ayer and P.M. Machmeier, Transmission Electron Microscopy Examination of Hardening and Toughening Phenomena in Aermet 100, *Metall. Trans. A*, Vol 24, 1993, p 1943
9. L. Chang, G.D.W. Smith, and G.B. Olson, Aging and Tempering of Ferrous Martensites, *J. Physique*, C2, T47, 1986, p 265
10. H.M. Lee, A.J. Garratt-Reed, and S.M. Allen, Composition of M_2C Phase in Tempering of High Co-Ni Steels, *Scr. Metall.*, Vol 25, 1991, p 685
11. G.B. Olson, T.J. Kinkus, and J.S. Montgomery, APFIM Study of Multicomponent M_2C Carbide Precipitation in AF1410 Steel, *Surf. Sci.*, Vol 246, 1991, p 238
12. H.M. Lee, S.M. Allen, and M. Grujicic, Coarsening Resistance of M_2C Carbides in Secondary Hardening Steels: Part II. Alloy Design Aided by a Thermochemical Database, *Metall. Trans. A*, Vol 22, 1991, p 2869
13. H.M. Lee and S.M. Allen, Coarsening Resistance of M_2C Carbides in Secondary Hardening Steels: Part III. Comparison of Theory and Experiment, *Metall. Trans. A*, Vol 22, 1991, p 2877
14. G.B. Olson, "Overview: Science of Steel," *Innovations in Ultrahigh Strength Steel Technology*, Proc. 34th Sagamore Army Materials Research Conference, G.B. Olson, M. Azrin, and E.S. Wright, Ed., U.S. Army Materials Technology Laboratory, Watertown, MA, 1990, p 3
15. P.M. Machmeier, T. Matuszewski, R. Jones, and R. Ayer, Effect of Chromium Additions on the Mechanical and Physical Properties and Microstructure of Fe-Co-Ni-Cr-Mo-C Ultra-High Strength Steel: Part I, *J. Mater. Eng. Perform.*, Vol 6 (No. 3), 1997, p 279-288
16. M. Avrami, Kinetics of Phase Change, I, *J. Chem. Phys.*, Vol 7, 1939, p 1103
17. M. Avrami, Kinetics of Phase Change, II, *J. Chem. Phys.*, Vol 8, 1940, p 212
18. M. Avrami, Granulation, Phase Change, and Microstructure, III, *J. Chem. Phys.*, Vol 9, 1941, p 177
19. W.A. Johnson and R.F. Mehl, Reaction Kinetics in Processes of Nucleation and Growth, *Trans. AIME*, Vol 135, 1939, p 146
20. C. Wert and C. Zener, Interference of Growing Spherical Precipitate Particles, *J. Appl. Phys.*, Vol 21, 1950, p 5
21. P. Wilkes, The Kinetics of Alloy Carbide Formation in Ferrite, *Met. Sci.*, Vol 2, 1968, p 8
22. J.M. Derbyshire and J. Barford, "The Mechanism of Phase Transformation in Crystalline Solids," Monograph No. 33, London Institute of Metals, 1969, p 65
23. S. Murphy and J.A. Whiteman, The Kinetics of Mo_2C Precipitation in Tempered Martensite, *Met. Sci.*, Vol 4, 1970, p 58
24. T. Sakuma, N. Watanabe, and T. Nishizawa, The Effect of Alloying Element on the Coarsening Behavior of Cementite Particles in Ferrite, *Trans. JIM*, Vol 21, 1980, p 159
25. M. Lee, S.M. Allen, and M. Grujicic, Sagamore Army Materials Research Proceedings, ibid., p 127
26. J.S. Montgomery and G.B. Olson, Kinematics of M_2C Carbide Precipitation, Sagamore Army Materials Research Proceedings, ibid., p 147
27. G.M. Carinci, et al., AF/FIM Study of Multicomponent M_2C Precipitation, Sagamore Army Materials Research Proceedings, ibid., p 179
28. R.A. Vandemeer and B.B. Rath, Kinetic Theory of Recrystallization, *Recrystallization*, TMS-AIME, 1990, p 49
29. J.S. Langer and A.J Schwartz, Kinetics of Nucleation in Near-Critical Fluids, *Phys. Rev. Lett.*, Vol 21, 1980, p 948
30. I.M. Lifshitz and V.V. Slyozan, The Kinetics of Precipitation from Supersaturated Solid Solutions, *J. Phys. Chem. Solids*, Vol 19, 1961, p 35
31. H. Wendt and P. Haasen, "Nucleation and Growth of γ'-Precipitates in Ni-14 at% Al," *Acta Metall.*, Vol 31 (No. 10), 1983, p 1649
32. G.W. Greenwood, Particle Coarsening, the Mechanism of Phase Transformations in Crystalline Solids, *Acta Metall.*, Vol 31 (No. 10), 1983, p 103